

GPS Receiver Architecture and Expected Performance for Autonomous Navigation in High Earth Orbits

MICHAEL C. MOREAU and PENINA AXELRAD

Colorado Center for Astrodynamics Research, University of Colorado at Boulder, Boulder, Colorado

JAMES L. GARRISON*

Purdue University, West Lafayette, Indiana

ANNE LONG

Computer Sciences Corporation, Lanham-Seabrook, Maryland

Received April 2000; Revised July 2000

ABSTRACT: *GPS is an enabling technology for autonomous spacecraft navigation, including mission concepts involving formation flying in highly eccentric orbits. However, to date most spaceborne GPS applications have been limited to low earth orbits or postprocessing applications. This paper describes the problems associated with using GPS in the high earth orbit (HEO) environment and presents a GPS receiver design optimized for these applications. The design builds upon the PiVoT receiver developed by Goddard Space Flight Center by incorporating the GPS Enhanced Orbit Determination (GEODE) navigation filter, a high-quality clock, and enhancements to basic receiver acquisition and tracking algorithms. Predicted navigation performance for several representative missions, including geosynchronous and geosynchronous transfer orbits, is presented. The analysis shows that a modest reduction in the acquisition threshold of the receiver enables reliable navigation performance even in very high orbits with unfavorable antenna placement restrictions.*

INTRODUCTION

The prospect of using GPS for autonomous navigation of satellites in highly eccentric and geosynchronous orbits has been considered for some time, with the goal of increasing spacecraft autonomy and reducing operations costs. Recently, researchers have started developing satellite missions in these high earth orbits (HEOs) that require on-board orbit information for formation flying and coordination of multiple spacecraft. GPS is considered to be an enabling technology for these mission concepts [1]. Table 1 provides a sample of HEO missions currently under development or proposed

for flight within this decade. These missions demonstrate the growing number of spacecraft that stand to benefit from a GPS tracking capability at high altitudes. The wide variety of mission concepts, orbits, and pointing strategies listed hints at the broad challenges faced in applying GPS to these missions.

GPS has been used extensively for satellites in low earth orbit (LEO), and several commercial receivers exist that can provide reliable and efficient on-board navigation solutions [13, 14]. In their current form, these receivers are not directly applicable to HEO missions because of important differences in the vehicle dynamics, signal levels, and geometric coverage. Many existing GPS receivers would have difficulty forming a single point solution in HEO, and could by no means reliably provide an autonomous navigation capability in these orbits. A receiver designed specifically for the conditions present in HEO will enable the application of GPS to these missions without relying on enhance-

* During the period when this work was performed, Dr. Garrison was affiliated with NASA Goddard Space Flight Center, Greenbelt, Maryland.

Table 1 — HEO Communications and Scientific Missions Proposed or Under Development

Mission	Spacecraft/Orbit Description	Notes
IMAGE (Imager for Magnetopause-to-Aurora Global Exploration) [2]	1000 km \times 7 R _E altitude orbit	Magnetospheric science mission Launched: March 25, 2000
Cluster II [3]	3 R _E \times 18.6 R _E altitude orbit	Science mission Four spacecraft flying in formation Launched: July 2000
AMSAT Phase 3D [4]	4000 \times 42,000 km altitude orbit	Communications satellite Launched: November 2000
STENTOR [5]	Geosynchronous	Launch: late 2000
IMEX (Inner Magnetosphere Explorer) [6]	350 \times 35,800 km altitude orbit	Science mission Launch: mid-2001
AMM (Auroral Multiscale Midex mission) [7]	600 \times 7000 km altitude	Four spacecraft flying in formation Launch: 2002
Ellipso [8]	Three orbital planes: Two - 633 \times 7605 km One - 8050 km circular	Mobile communications 14 + 3 satellites in three orbital planes Operational: 2002
Nanosat Constellation Trailblazer (ST5) [9]	Three orbits under consideration: A) 500 \times 35,700 km altitude B) 3500 \times 35,700 km altitude C) 2 \times 9 R _E km altitude	Technology validation mission Three spacecraft flying in formation Launch: 2003
Auroral Lite [10]	1000 \times 8000 km altitude	Launch: 2004 (earliest)
Magnetospheric Multiscale (MMS) [11]	Four mission phases: 1200 km \times 11 R _E altitude 1200 km \times 29 R _E altitude 7 \times 79 R _E altitude 9 \times 49 R _E altitude	Five spacecraft flying in formation Launch: 2005–2006
Magnetospheric Constellation [12]	3 R _E perigee, 12-42 R _E apogee	50–100 satellites flying in formation Launch: ca. 2010
Inner Magnetosphere Constellation Mission or Orion Constellation Mission (part of Magnetospheric Constellation) [12]	Three 1 \times 5.5 R _E altitude orbits with 10 spacecraft each Three 1 \times 11 R _E altitude orbits with 4 spacecraft each	Science mission 42 spacecraft in 6 orbital planes

ments to the existing GPS constellation. This paper describes ongoing work to develop a GPS receiver that will enable autonomous navigation for many of the missions listed in Table 1. An overview of the HEO GPS receiver architecture is presented, followed by simulation results for expected GPS signal visibility and navigation accuracies for several mission scenarios.

BACKGROUND

The high altitudes reached by HEO spacecraft present a very unfavorable environment for the reception of GPS signals. The most significant difference from LEO is the sparse nature of GPS signals at high altitudes. There are rarely four or more satellites present simultaneously, the condition required for a GPS receiver to produce an instantaneous point solution for position and time.

Furthermore, the available signals are generally very weak and originate from only a small region of the sky. This environment stresses both the ability of the receiver to acquire and track the signals and the quality of the navigation solution obtained. Numerous papers appearing in recent years have examined the problem of receiving GPS signals in highly eccentric or geostationary orbits [15–17]. In our analysis, a GPS satellite is considered currently “visible” if the line of sight (LOS) to the satellite is unobstructed and the power level at the receiver is sufficient for signal acquisition and tracking. The major factors affecting GPS signal visibility in HEO are summarized below.

The main beam of the transmitted GPS signals is approximately 21.3 deg wide (half-angle) and is directed at the center of the earth. Because the earth subtends a half-angle of only 13.9 deg, there is approximately 8 deg of signal spillover [18]. Fig-

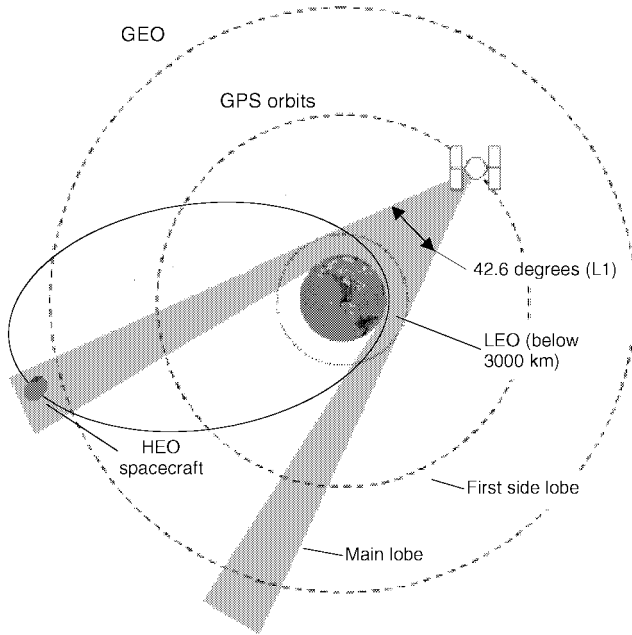


Fig. 1 – Geometry for Reception of GPS Signals by a HEO Spacecraft

Figure 1 illustrates the geometry for tracking these limb-crossing GPS signals by a receiver high above the altitude of the GPS constellation. The only GPS signals reaching the receiver at these high altitudes originate from satellites on the opposite side of the earth. Figure 1 shows that the limit of the main beam corresponds to a limb-crossing altitude of approximately 3000 km, above which the GPS signal visibility begins to drop off rapidly. The figure also shows the first side lobes radiating from the GPS satellites. The side lobe signals are generally about 20 dB lower power than signals transmitted from the main beam; however, it is possible that a receiver could actually track a GPS satellite from these side lobe signals when the geometry is favorable.

Below 3000 km altitude, signals from 10 or more GPS satellites are typically present with the current GPS constellation, reaching the receiver with nearly uniform power levels and geometric distribution above the local horizon. Other than the high Doppler shifts and the frequent rising and setting of GPS satellites, this is not unlike the visibility for terrestrial GPS users. Any orbit in which the spacecraft remains within this good GPS visibility region below 3000 km is considered LEO in the context of this paper. However, above 3000 km altitude, the conditions for receiving GPS signals become much less favorable. Received signal power typically decreases because (1) the transmitted power of some

signals drops off as a result of the attenuation pattern of the transmitting GPS satellite, and (2) the ranges to many of the visible GPS satellites increase. As a result, the received power levels of signals from many of the GPS satellites geometrically in view are below the tracking threshold of the receiver.

For medium altitudes, roughly between 3000 km and the 20,000 km altitude of the GPS constellation, signal visibility is already significantly reduced compared with a LEO; however, the signals present can originate from any part of the sky. At altitudes above 20,000 km, visible signals radiate from a narrow cone centered in the direction of the earth, there are rarely four or more GPS signals present simultaneously, and GPS signal outages lasting several hours are not uncommon. Several factors further complicate high-altitude GPS operations. Occasionally, a single, powerful signal from a GPS satellite at close range will jam all the other signals being tracked by the receiver, causing loss of lock and a data outage. Through perigee passage of a highly eccentric orbit, the relative LOS velocities (Doppler) will be at times greater than ± 10 km/s (± 52.5 kHz). Some missions may employ pointing strategies that preclude mounting GPS antennas in the most favorable orientations for receiving GPS signals, further reducing signal visibility. Finally, the radiation environment for HEO spacecraft can be orders of magnitude more severe than in LEO.

Clearly, as spacecraft altitude increases, the conditions for tracking GPS signals become less favorable, and existing GPS receivers will not function properly. Nevertheless, several flight experiments launched in 1997 demonstrated limited high-altitude tracking of both the GPS main lobe and side lobe signals in highly elliptical orbits using existing GPS technology [19-21]. These early experiments provided a proof of concept for the tracking of GPS signals at high altitudes, and even the tracking of GPS side lobe signals; however, they did not demonstrate a real-time autonomous navigation capability. A paper appearing in 1988 outlined technological approaches to improve the availability of GPS signals in a GEO orbit [22]. Since then, several groups have undertaken efforts to develop new GPS receivers that can function in high-altitude orbits. Most notably, the French Space Agency (CNES) recently demonstrated weak GPS signal tracking techniques that achieve significant tracking threshold reductions in the GPS receiver [23]. The objective of this research project is to develop a GPS receiver that incorporates the necessary design changes and enhancements to provide a reliable autonomous navigation capability in HEO orbits.

HEO RECEIVER ARCHITECTURE

The following is an overview of the systems-level requirements for an HEO GPS receiver, above and beyond the capabilities that would typically be required of a GPS receiver operating in LEO.

On-Board Navigation Filter

A capable and robust navigation filter and clock model are required to enable the receiver to generate solutions when fewer than four satellites are visible simultaneously and to propagate a solution through long GPS signal outages. The filter must support rapid reinitialization for missions that may require the receiver to be turned off occasionally to conserve power. Most heritage space receivers have at best a crude internal orbit propagator for this purpose [24].

Traditionally, clock performance in space GPS receivers has not been of great concern because clock bias is part of the traditional point solution. An accurate and stable receiver clock becomes very important for the HEO/GEO receiver because it will be required to operate for long periods of time when fewer than four GPS signals are available and a traditional point solution is not possible. The clock stability and the ability to model the clock in the navigation filter will have a significant impact on the overall performance of the receiver.

Optimized Receiver Algorithms

It is necessary to make some changes to algorithms traditionally employed in the signal acquisition and tracking functions in the receiver to cope with the conditions in HEO. Criteria other than traditional dilution of precision (DOP) or highest elevation must be used to select and assign satellites to receiver channels for tracking. An estimate of carrier-to-noise spectral density ratio (C/N_0) should be used as one of the satellite selection criteria. The signal acquisition algorithms may require mission-specific customizations and must be robust enough to handle the varying conditions (e.g., Doppler, C/N_0) experienced over each orbit. Furthermore, the search pattern used to vary code delay and Doppler frequency to look for new satellites must take into account the expected range of Doppler frequencies encountered in these orbits. One potential way to speed up this search is to assign multiple correlator channels to one satellite at different Doppler frequencies.

Specific strategies can be employed to increase the number of GPS signals visible under certain conditions by better enabling the receiver to track weak GPS signals and to take advantage of available side lobe signals. Optimizing the tracking loop

design for the expected dynamics of HEO and exploiting the navigation and clock information contained in the navigation filter will produce some improvement in tracking weaker GPS signals and will result in improved navigation performance. At the same time, the receiver must be tolerant of jamming conditions that periodically arise in HEO. The near-far problem could cause loss of tracking due to jamming from another GPS space vehicle in close proximity.

Robust and Flexible Hardware

The changing geometric distribution of signals in the sky throughout an orbit requires multiple antennas and antenna orientations to provide the best coverage. The receiver should allow dynamic assignment of correlator channels to antennas to make the best use of the resources in the receiver as conditions change over the course of the mission, or even during each orbit. Certain nadir-pointing spacecraft can use high-gain receiving antennas to improve signal visibility at high altitudes when the GPS signals are all concentrated in one portion of the sky. Radiation-hardened components, box-level shielding, and single event upset (SEU)-tolerant software will be required for the receiver to survive the extremely severe radiation environment in high-altitude orbits.

NASA Goddard Space Flight Center (GSFC) is currently developing a new space GPS receiver called PiVoT for use on a wide range of future earth-orbiting spacecraft, including HEO missions similar to those outlined in Table 1. PiVoT is based upon the MITEL 2010/2021 chipset and utilizes an open architecture design employing an industry standard bus, which allows the use of different processors and possible expansion of the number of radio frequency (RF)/correlator boards. At present, the design supports up to 24 correlator channels with as many as four RF inputs. The PiVoT clock is a high-quality temperature-controlled crystal oscillator with a specified root Allan variance better than 0.4×10^{-10} for 1 s. The GPS Enhanced Orbit Determination (GEODE) software will be incorporated as a real-time navigation filter in the PiVoT receiver. Initially developed for LEO applications, GEODE consists of an extended Kalman filter, a high-fidelity model of the orbital dynamics, and fault detection capabilities [25]. A new version of the GEODE software currently under development will have the capability of estimating relative states between multiple spacecraft flying in formation, a requirement of several of the missions listed in Table 1.

The existing capabilities of the PiVoT receiver, including an integrated navigation filter, a good clock, and flexible hardware and software design,

make it an excellent candidate for an HEO GPS receiver. Work is ongoing to develop and implement the necessary capabilities in PiVoT to address the remaining HEO requirements identified above. This work involves primarily enhancements to receiver algorithms that will enable operation in all HEO orbits, and can be separated into four key elements: (1) GPS signal visibility and dynamics and systems design, (2) coupling of Kalman filter state estimator with tracking loop functions, (3) satellite selection and signal acquisition algorithms, and (4) tracking loop optimization for tracking of weaker GPS signals.

The tracking threshold has an important impact on GPS receiver performance in HEO applications because of the weaker signals associated with these orbits. Previous analytical studies of GPS visibility in HEO have indicated a significant number of GPS observations present at signal levels just below the tracking threshold of current receivers. By optimizing the tracking loop design for the predictable dynamics associated with HEO missions and by taking advantage of the capabilities of GEODE, modest improvements in the tracking threshold of 5 to 7 dB are achievable. GPS signal visibility and navigation simulation results are presented that show the potential improvements from modest re-

ductions in the tracking threshold over that of a conventional receiver.

SIMULATION OVERVIEW

Four scenarios, each corresponding to a specific orbit, spacecraft attitude profile, GPS antenna configuration, and other mission parameters, have been created based on some key missions listed in Table 1. The scenario specifications are summarized in Table 2. HEO1-A and HEO1-B are based on the orbit and mission design of the IMEX spacecraft, a spin-stabilized spacecraft in a geostationary transfer orbit with a low perigee, and apogee close to the geostationary altitude. Two hemispherical GPS antennas are assumed, aligned parallel and antiparallel to the spin axis to provide full sky coverage. These scenarios were chosen to illustrate two different points in the IMEX mission as the orientation of the spin axis, and consequently the GPS antennas, changes. Because the spacecraft pointing requirements preclude the GPS antennas from being oriented in the most favorable direction (nadir) for receiving GPS signals at high altitudes, these two scenarios compare favorable (HEO1-A) and unfavorable (HEO1-B) orientations of the GPS

Table 2 — Scenario Specifications

Parameter	HEO1-A	HEO1-B	HEO2	GEO1
	Geostationary Transfer Orbit, Antennas Favorably Aligned	Geostationary Transfer Orbit, Antennas Not Favorably Aligned	$3 \times 10 R_E$ (very high altitude) Eccentric Orbit	Geostationary Orbit with High-Gain, Nadir-Pointing GPS Antenna
Orbital Period (h)	10.5	10.5	23.5	24.0
Perigee Altitude (km)	349	349	12756	35777
Apogee Altitude (km)	35800	35800	57402	35797
Semimajor Axis (km)	24446.0	24446.0	41457.0	42165.5258
Eccentricity	0.7248	0.7248	0.53846	0.000242
Inclination (deg)	26.4	26.4	28.5	0.25
Argument of Perigee (deg)	137.0	107.0	0.0	324.1
Ascending Node (deg)	358.0	358.0	90.0	95.1
Mean Anomaly (deg)	0.0	0.0	0.0	33.4
Epoch Date	02/09/99 04:10:00	10/10/98 05:20:00	06/21/98 00:00:00	06/21/98 00:00:00
Spacecraft Mass	160 kg	160 kg	10 kg	2100 kg
Cross-Sectional Area	1.5 m^2	1.5 m^2	0.1 m^2	54 m^2
Antenna 1 Config.	Hemispherical antenna with boresight parallel to spin axis	Hemispherical antenna with boresight parallel to spin axis	Hemispherical antenna with boresight parallel to spin axis	Nadir-pointing high-gain antenna
Antenna 2 Config.	Hemispherical antenna with boresight antiparallel to spin axis	Hemispherical antenna with boresight antiparallel to spin axis	Hemispherical antenna with boresight antiparallel to spin axis	None
Spacecraft Attitude	Spin axis parallel to earth-sun vector	Spin axis parallel to earth-sun vector	Spin axis perpendicular to ecliptic plane	Three-axis stabilized, earth-pointing

antennas that will occur at different points during a typical mission similar to IMEX.

The HEO2 scenario is based on one of the proposed orbits for the Nanosat Constellation Trailblazer Mission (ST5). HEO2 is a more difficult orbit from a GPS visibility standpoint because both the perigee and apogee altitudes are much higher than for HEO1. HEO2 also features a spinning spacecraft with two hemispherical antennas not necessarily oriented favorably for receiving GPS signals. The final scenario discussed, GEO1, features a geostationary orbit based on the GOES-10 spacecraft. For this scenario, a single high-gain, nadir-pointing GPS antenna is assumed to take advantage of the nadir-pointing attitude of the satellite. Figure 2 illustrates the relative size and shape of the three orbits described above. Note that except near perigee of the HEO1 scenarios, the spacecraft are never within the good GPS visibility region below 3000 km altitude.

These scenarios were selected to compare visibility and navigation performance for a range of missions. For each scenario, three simulated GPS datasets were produced, corresponding to assumed receiver tracking thresholds of 35 dB-Hz (nominal), 30 dB-Hz (5 dB improvement), and 28 dB-Hz (7 dB improvement), in order to assess the improvement in performance resulting from modest reductions in the tracking threshold. The baseline tracking threshold assumed in this paper for a conventional, unmodified receiver was 35 dB-Hz, which was based on tracking thresholds appearing in the literature for other GPS receivers [17, 26] and experimental tests of the tracking performance of the MITEL hardware using a static receiver tracking GPS

satellites from a rooftop antenna. The simulated pseudorange measurements were then processed using GEODE to evaluate the expected navigation performance for each dataset.

SIMULATION PROCEDURE

The following procedure was used to generate each set of simulated GPS pseudorange measurements:

1. Truth ephemeris for each host satellite was generated using the Goddard Trajectory Determination System (GTDS) with the high-accuracy force model parameters listed in Table 3. GTDS is the primary orbit determination program used for operational satellite support at GSFC [27].
2. GPS satellite orbits were generated using the actual broadcast ephemeris for the simulation epoch listed in Table 4.
3. Realistic GPS pseudorange measurements were generated using the computed ephemeris and the GPS measurement and error model simulation parameters listed in Table 4. A GPS signal was considered visible and a pseudorange measurement generated for it if the following conditions were satisfied:
 - Geometric LOS to the GPS satellite is not obstructed by the earth.
 - The LOS lies within predetermined antenna elevation mask angles (for transmitter and receiver) and does not cross below a predetermined atmospheric mask altitude above the earth's surface.
 - Received signal power is above the receiver acquisition threshold.
 - Twelve receiver channels are assumed; when more than 12 GPS satellites are visible simultaneously, the signals with the highest C/N_0 are selected for tracking.

Selective Availability (SA) measurement errors were applied at a 25 m (1σ) level, using the Lear4 autoregressive integrated moving-average time-series model [28]. For GPS signals crossing the earth's limb, ionospheric delays were modeled us-

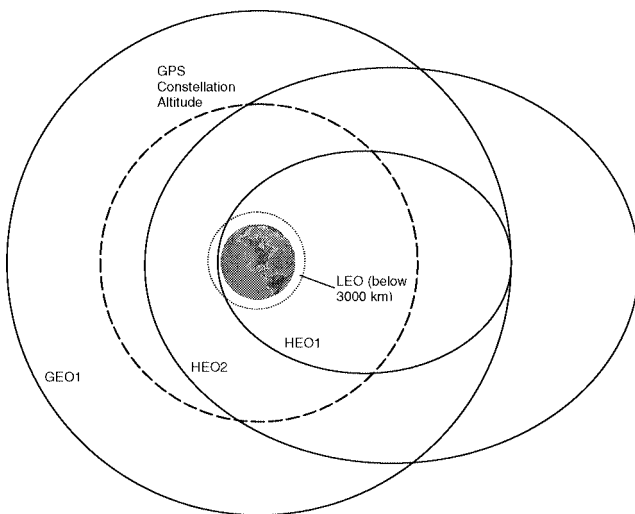


Fig. 2 – Comparison of Simulated Orbits (When the spacecraft is near apogee, the ideal user antenna orientation is nadir to receive signals crossing the limb of the earth. If user antennas are not aligned with nadir (such as for HEO1-B and HEO2), reduced signal visibility will result.)

Table 3 — HEO Truth Ephemeris Force Model Parameters

Parameter	Value
Nonspherical earth gravity model	70 × 70 Joint Goddard Model (JGM)-3
Solar and lunar ephemerides	Jet Propulsion Laboratory Definitive Ephemeris (DE) 200
Spacecraft area model	Spherical
Solar radiation pressure coefficient	1.4

Table 4 — GPS Measurement and Error Model Simulation Parameters

Parameter	Value
Measurement data rate	60 s
GPS satellite ephemerides	Broadcast ephemeris for June 21–26, 1998
GPS satellite characteristics	
SA errors	25 m (1 σ)
Transmitting antenna pattern	Nominal GPS L-band antenna pattern, modeled to a beamwidth of 90 deg (half-angle) [30]
Transmitted power	28.0 dBW in maximum gain direction
User antenna model:	
Hemispherical antenna	Maximum gain: 4.9 dBic Horizon mask: 90 deg from boresight
High-gain antenna	Maximum gain: 9.2 dBic Horizon mask: 56 deg from boresight
GPS receiver characteristics	
Receiver acquisition threshold	35, 30, or 28 dB-Hz
Receiver system losses	2.9 dB
System noise temperature	Earth-pointing antenna: 290K Otherwise: 180K
Visibility constraints	12 channels with GPS satellite signals selected based on highest signal-to-noise ratio Earth blockage, with 50 km altitude atmospheric mask Transmitting antenna beamwidth and receiving antenna horizon masks Received C/N_0 above tracking threshold
Ionospheric delays	Exponential function of height of ray path (HORP) above earth's surface
Receiver clock bias white noise spectral density	$9.616 \times 10^{-20} \text{ s}^2/\text{s}$
Receiver clock drift rate white noise spectral density	$1.043 \times 10^{-27} \text{ s}^2/\text{s}^3$
Random pseudorange errors	2 m (1 σ)

ing an exponential function of the height of ray path (HORP) above the earth, which was based on ionospheric delays computed for each test orbit using the Bent ionospheric model [27]. Receiver clock noise was simulated assuming a very high-stability crystal oscillator with a 1 s root Allan variance of 0.16×10^{-9} . This value is approximately an order of magnitude more conservative than the manufacturer's 1 s specification for the oscillator that will be used in the PiVoT receiver. A twice-integrated random walk model was used to simulate the clock bias and clock drift noise contributions [29].

The simulated GPS pseudorange measurements were processed using GEODE, subject to the processing parameters provided in Table 5. A Monte Carlo error analysis was performed for each orbital scenario and acquisition threshold. Ensemble error statistics for the navigation state estimates were computed based on 50 sets of simulated pseudorange measurements. For each measurement set, all random errors in the simulation (SA, noise, and clock) were reinitialized using a different seed value.

The following sections describe the Monte Carlo and satellite visibility results.

SIGNAL VISIBILITY RESULTS

GPS signal visibility results are presented in Figures 3 through 6 and are summarized in Table 6. The number of visible GPS signals at 35, 30, and 28 dB-Hz thresholds is plotted versus time for each orbital scenario. In each case, the number of visible signals contributed by side lobe radiation from the GPS satellites is indicated. Several common observations can be made for all of the scenarios considered. The visibility is shown over a minimum of two orbital periods for each scenario. In every case, the reduction in the acquisition threshold of the receiver results in an increase in the number of visible GPS signals and a corresponding increase in the number of GPS observations that can be recorded. This is demonstrated by the increase in the percentage of time one or more, or four or more, GPS satellites are visible as given in

Table 5 — GEODE Processing Parameters

Parameter	Value
Nonspherical earth gravity model	30 × 30 Joint Goddard Model (JGM)-2
Solar and lunar ephemeris	Low-precision analytical ephemeris
Initial position error in each component	100 m (consistent with point solution accuracy under SA conditions)
Initial velocity error in each component	1 m/s (consistent with point solution accuracy)
Initial receiver time bias error	100 m
Initial receiver time bias rate error	0.1 m/s
Initial solar radiation pressure coefficient error	HEO: 0.6 (40%) GEO: 0.042 (3%)
Estimated state	<ul style="list-style-type: none"> • User position and velocity in J2000 • GPS receiver time bias and time bias drift • Solar radiation pressure coefficient
GPS satellite ephemerides	Broadcast ephemeris for June 21–26, 1998
Ionospheric editing	500 km minimum limb-crossing altitude
Measurement processing rate	HEO2: 180 s GEO1: 60 s

Table 6. In highly eccentric orbits in which the altitude of the spacecraft changes greatly, the visibility is best at perigee and worst near apogee, as can clearly be seen in the plots provided in Figures 3, 4, and 5.

The differences between HEO1-A and HEO1-B shown in Figures 3 and 4 are attributed solely to the fact that the GPS antennas are oriented less favorably, i.e., more off-nadir in HEO1-B. As noted in Table 6, the mean off-nadir angle of the GPS antenna at apogee is 5.2 deg for HEO1-A and

85.1 deg for HEO1-B. Thus for HEO1-B, the signals are received at low elevation angles on the receiving antenna, and reduced visibility results. The low perigee altitude of the HEO1 orbit (350 km) means that four or more satellites are visible, and consequently point solutions are possible for several hours of each orbit.

The visibility for the HEO2 scenario, shown in Figure 5, is significantly poorer than for either HEO1 case. Signal visibility is inherently poorer because HEO2 is a much higher orbit, and it is

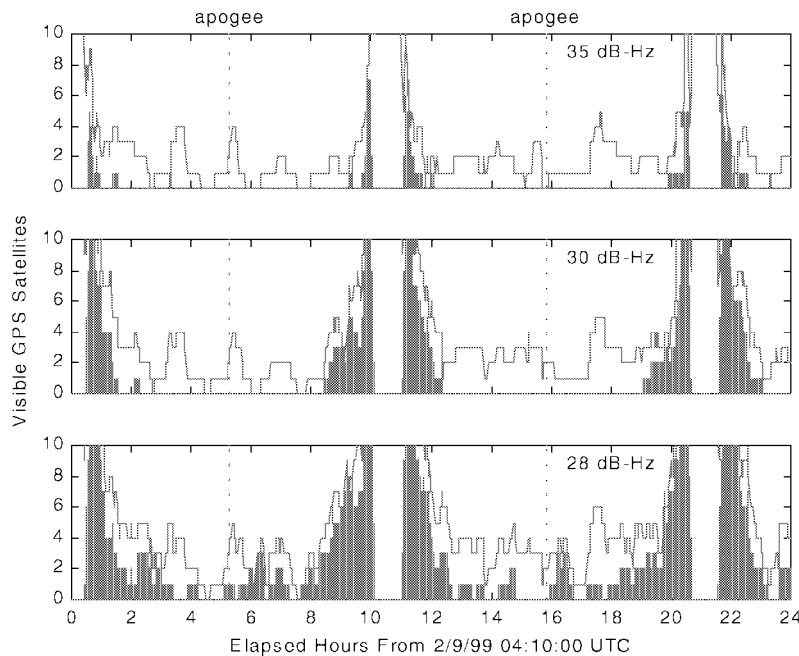


Fig. 3 – Total GPS Signal Visibility (solid line) and Contribution from GPS Side Lobes (shaded) for HEO1-A Scenario, Which Has a Favorably (nadir) Pointed Antenna Near Apogee (The first plot shows the number of visible GPS satellites during a period of just over two orbits corresponding to a 35 dB-Hz tracking threshold. The next two plots show that as the tracking threshold is reduced to 30 and 28 dB-Hz, respectively, the result is an increase in the number of visible satellites.)

Table 6 — Summary of GPS Signal Visibility Results

Scenario	Antenna Off-Nadir Angle at Apogee (deg)	Threshold (dB-Hz)	Percent of Time One or More Satellites Visible	Percent of Time Four or More Satellites Visible
HEO1-A	5.2	35	90.0	24.0
		30	96.0	37.0
		28	98.7	59.0
HEO1-B	85.1	35	62.0	21.0
		30	82.0	34.0
		28	91.0	41.0
HEO2	66.6	35	44.0	6.0
		30	71.0	16.0
		28	78.0	22.0
GEO1	0.0	35	78.0	4.1
		30	98.9	60.3
		28	100.0	85.0

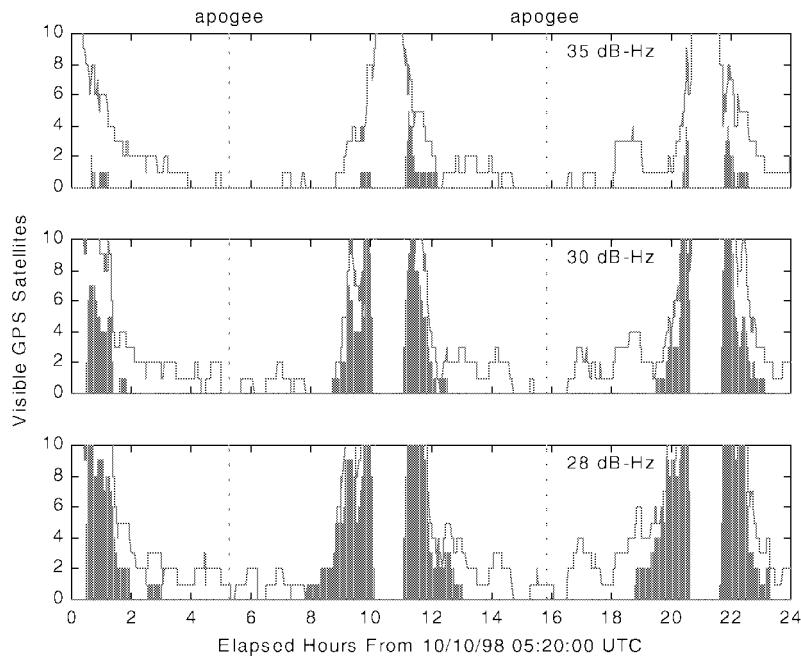


Fig. 4—Total GPS Signal Visibility (solid line) and Contribution from GPS Side Lobes (shaded) for HEO1-B Scenario, Which Has an Unfavorably (85 deg off-nadir) Pointed Antenna Near Apogee (The first plot shows the number of visible GPS satellites corresponding to a 35 dB-Hz tracking threshold. The next two plots show that as the tracking threshold is reduced to 30 and 28 dB-Hz, respectively, the result is an increase in the number of visible satellites.)

further reduced because the GPS antenna is approximately 66 deg off-nadir at apogee. Even at perigee, point solutions are rarely possible (less than 6 percent of the time).

Unlike the previous scenarios, the spacecraft in the GEO1 scenario shown in Figure 6 maintains a constant distance from the earth. Additional signal space loss is compensated at the geostationary altitude by an additional 6 dB of signal gain using a high-gain, nadir-pointing GPS antenna. Thus signal visibility for this scenario is improved by exploiting the nadir-pointing spacecraft attitude, in

which only a narrow antenna beamwidth is needed to cover the region of space from which the GPS signals radiate. For the GEO1 scenario, the reduction in the tracking threshold dramatically increases the amount of time four or more satellites are visible simultaneously.

NAVIGATION RESULTS

Navigation results for HEO2 and GEO1, the two scenarios with the poorest GPS signal visibility, are summarized in Table 7. The navigation errors were

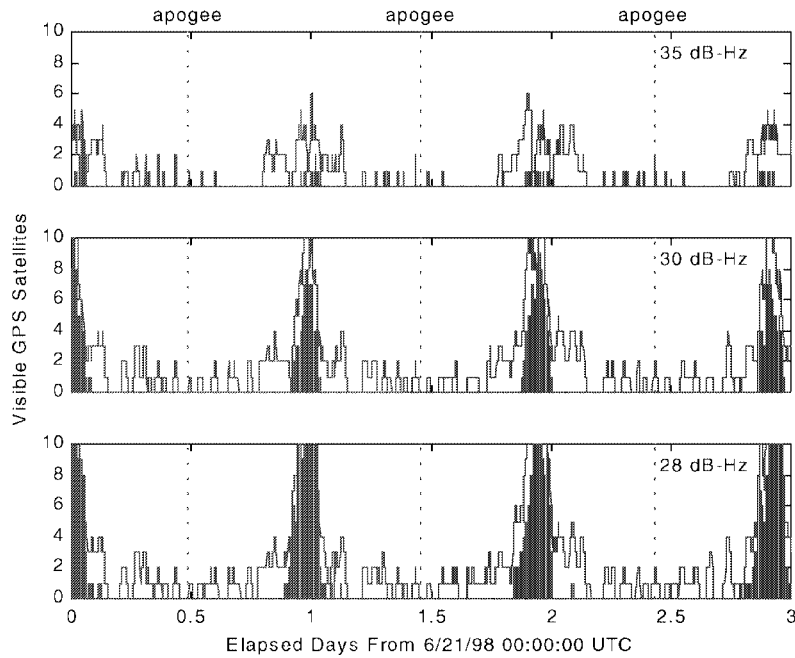


Fig. 5 – Total GPS Signal Visibility (solid line) and Contribution from GPS Side Lobes (shaded) for HEO2 Scenario, Which Has an Antenna Oriented 66 deg Off-Nadir Near Apogee (The plots show the number of visible GPS satellites over a 3 day period, first corresponding to a 35 dB-Hz tracking threshold, followed by thresholds of 30 and 28 dB-Hz.)

computed by differencing the truth and estimated state vectors.

Figures 7 and 8 compare the HEO2 ensemble true root-mean-squared (RMS) errors for the three receiver acquisition thresholds for position and velocity. The ensemble true RMS error, which is defined as the RMS of the true error (difference be-

tween the estimated and true state) at each time, t , computed across all 50 Monte Carlo solutions, is computed as follows:

$$R_n(t) = \sqrt{\left(1 - \frac{1}{n}\right) \sigma_n^2(t) + \bar{x}_n^2(t)}$$

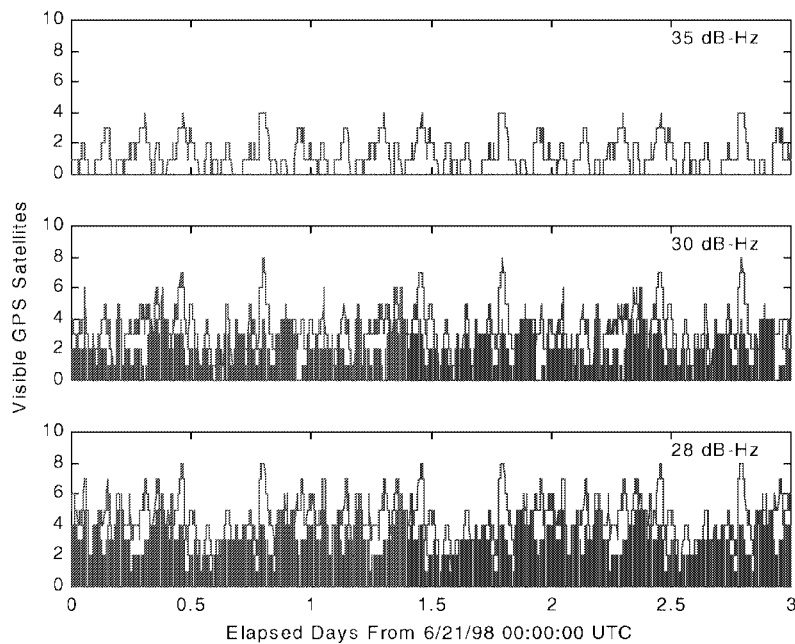


Fig. 6 – Total GPS Signal Visibility (solid line) and Contribution from GPS Side Lobes (shaded) for GEO1 Scenario, Which Has a Single High-Gain, Nadir-Pointing Antenna (The plots show the number of visible GPS satellites over a 3 day period, first corresponding to a 35 dB-Hz tracking threshold, followed by thresholds of 30 and 28 dB-Hz.)

Table 7 — Summary of Steady-State Navigation Errors

Scenario	Threshold (dB-Hz)	RMS Position Error (m)	RMS Velocity Error (mm/s)	RMS Clock Bias Error (m)
HEO2	35	30.0	2.0	17.0
	30	20.0	1.2	12.0
	28	18.0	1.1	10.5
GEO1	35	15.0	1.0	6.0
	30	6.0	0.4	3.0
	28	5.0	0.35	2.5

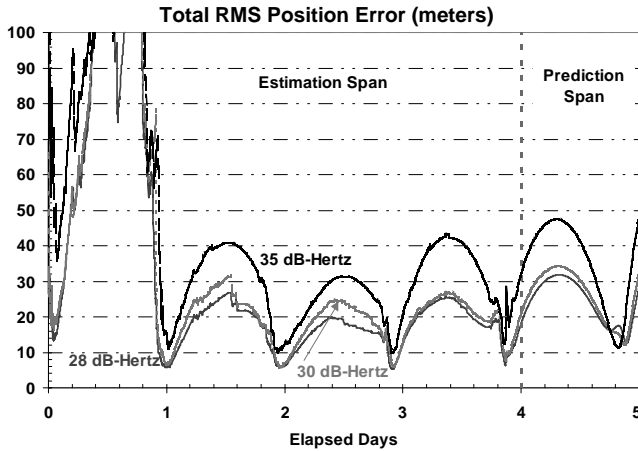


Fig. 7—Ensemble RMS Position Errors for HEO2 (The steady-state error statistics shown in Table 7 were computed using data after the first orbit.)

where $x_n(t)$ is the true error for the n th simulation, n is 50, and

$$\bar{x}_n(t) = \frac{1}{n} \sum_{i=1}^n x_i(t)$$

$$\sigma_n^2(t) = \frac{1}{n-1} \left(\sum_{i=1}^n x_i^2(t) - n\bar{x}_n^2(t) \right)$$

These results were obtained by processing measurements from all acquired GPS satellites every 3 min. Starting at perigee, approximately 1 orbit (23.5 h) of processing was required to achieve steady-state performance (i.e., filter has converged to a “minimum” error solution with a stable, consistent covariance estimate). Starting at apogee, two perigee passages were required to achieve steady-state performance. These analyses indicate that total position and velocity RMS accuracies of 30 m and 2 mm/s, respectively, can be achieved for the HEO orbit using a receiver with a high-stability oscillator and a signal acquisition threshold of 35 dB-Hz. The largest errors occur near apogee and the smallest errors near perigee, where the GPS visibility is better. Decreasing the signal acquisition threshold significantly reduces the total RMS

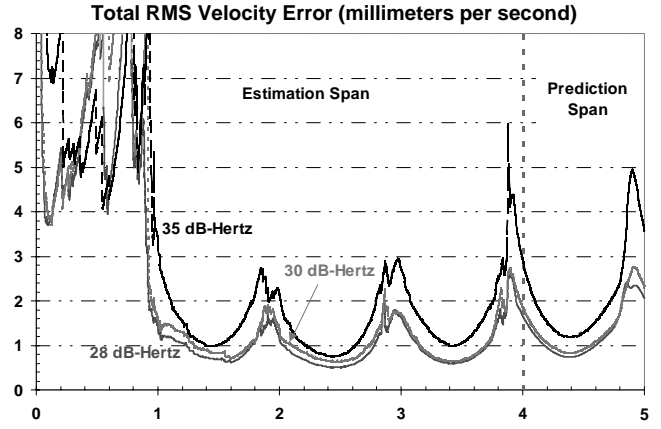


Fig. 8—Ensemble RMS Velocity Errors for HEO2 (The steady-state error statistics shown in Table 7 were computed using data after the first orbit.)

position and velocity errors, and improves the accuracy of the estimated clock bias.

Figures 9 and 10 compare the GEO1 steady-state ensemble true position and velocity RMS errors for the three acquisition thresholds over the 4.5 day estimation span and a 1 day prediction span. These results were obtained by processing measurements from all acquired GPS satellites every 1 min. These analyses indicate that total position and velocity RMS accuracies of about 15 m and 1 mm/s, respectively, can be achieved for the GEO orbit using a receiver with a high-stability oscillator and a signal acquisition threshold of 35 dB-Hz. Decreasing the signal acquisition threshold again reduces the total RMS position and velocity errors and improves the accuracy of the estimated clock bias.

The clock bias contributions to the pseudorange measurements were assumed to be correlated in time through the use of an integrated clock model. The 60 and 180 sampling intervals minimize the effects of the correlated SA measurement errors.

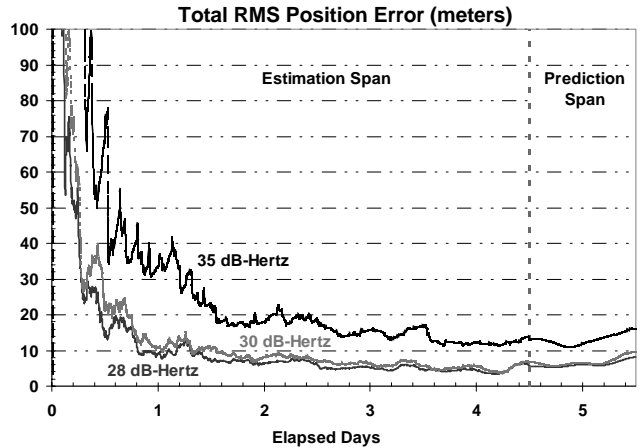


Fig. 9—Ensemble RMS Position Errors for GEO1 (The steady-state error statistics shown in Table 7 were computed using data after the first orbit.)

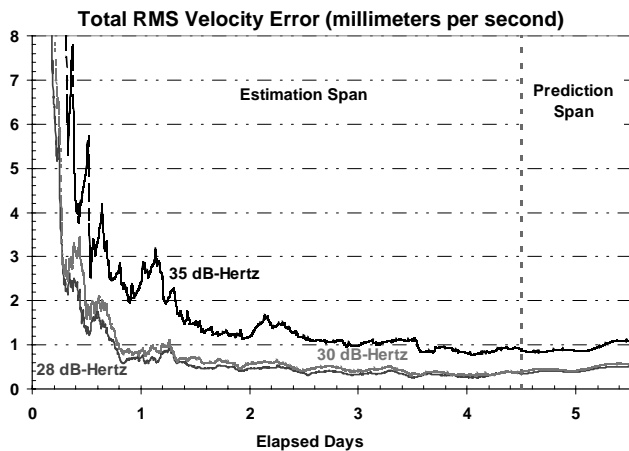


Fig. 10—Ensemble RMS Velocity Errors for GEO1 (The steady-state error statistics shown in Table 7 were computed using data after the first orbit.)

For both scenarios, GEODE was initialized assuming the initial state vector was obtained from a point solution computed by the GPS receiver, accurate to within 100 m and 1 m/s. A point solution requires simultaneous pseudorange measurements from a minimum of four GPS satellites. Inspection of HEO2 visibility (Figure 5) indicates that point solution computation would rarely be possible using a receiver with a 35 dB-Hz threshold and would be possible only near perigee with the lower thresholds. If a point solution is not available, the navigation filter can be initialized using a state vector estimated on the ground, propagated ahead in time, and uplinked to the satellite. This initialization scenario was simulated by applying initial position errors of 0.1, 1.0, and 0.3 km in the radial, in-track, and cross-track directions, respectively, and initial velocity errors of 1.0, 0.1, and 0.3 m/s in the radial, in-track, and cross-track directions, respectively. The larger initial errors had no significant impact on the steady-state navigation performance for any of the receiver threshold levels.

DISCUSSION

The primary factors affecting navigation performance for HEO satellites using a GPS receiver with a high-stability clock were found to be (1) the quality of GPS visibility, characterized by the number of GPS satellites that can be acquired simultaneously and the length of time when no GPS satellites can be acquired; (2) SA measurement errors; (3) large uncorrected ionospheric delays in the processed measurements; and (4) dynamic modeling errors. Based on the simulation models described, it is not surprising that SA was found to be the dominant error in the measurements. Navigation solution errors improved by more than 50 percent when SA errors were removed. The inclusion of measure-

ments with large ionospheric delays was the next-largest measurement-related contributor, producing significant biases in the clock bias estimates, particularly for the 35 dB-Hz acquisition threshold (29 m for HEO2 and 11 m for GEO1). The impact of random measurement error even at these low signal levels was much smaller than that of SA or ionospheric effects.

A sensitivity analysis was performed to assess the impact of dynamic modeling errors arising from unmodeled variations in the solar radiation pressure and errors in the predicted earth orientation parameters used in the transformation from the GPS earth-centered, earth-fixed coordinate frame to an inertial frame. The results indicated that when the solar radiation pressure force is a significant spacecraft perturbation, as is the case for many HEOs, the solar radiation pressure coefficient should be estimated in the filter to reduce this error. Furthermore, simulations for GEO1 using 30 day predicted values of the earth orientation parameters distributed by the International Earth Rotation Service show significant increases in the solution errors (about 15 m RMS), indicating that up-to-date values for the UT1-UTC time differences should be commanded on a weekly basis for best performance.

The performance of the orbit filter and the receiver tracking thresholds is very closely coupled. If the filter can consistently produce vehicle state estimates at the level of 100 m and 7 mm/s, it is possible to narrow the acquisition and tracking loop bandwidths and improve the tracking thresholds. This provides more observations to the filter, which clearly further improves the navigation performance. However, until the filter converges, errors in the propagated state can be quite large, and one might expect that no aiding can be provided to the tracking loops. In fact, even in this situation, one can use the known orbital dynamics and even a very crude estimate of the spacecraft position to aid the signal acquisition process.

The importance of an accurate and stable receiver clock was mentioned briefly earlier. The reason orbit determination systems are able to produce accurate results with sparse data is the predictable dynamics of a spacecraft in earth orbit. In this environment, the limitation on the state prediction process in the filter is the predictability of the oscillator. If oscillator rate variation is kept within the dynamic uncertainty of orbit propagation, there will be a benefit from even one satellite observation. If the oscillator is poor, one satellite does not provide much information about the orbit because all the information is essentially required to maintain clock information. The high-quality temperature-controlled crystal oscillator selected for the PiVoT receiver and modeled in these simulations ap-

proaches the best performance possible in a cost-constrained design.

To fully exploit the advantages of channel aiding based on navigation state estimates and receiver clock stability requires not only the robust design of the navigation filter, but a complete receiver system design optimized for the HEO environment, including satellite selection and signal acquisition algorithms, tracking loop design, antenna selection, and so on.

CONCLUSIONS AND FUTURE WORK

A GPS receiver architecture that will enable autonomous GPS navigation for HEO missions has been presented. Based on the PiVoT GPS receiver currently under development at GSFC, the HEO receiver will incorporate the GEODE navigation filter; a good clock; and enhancements to basic receiver algorithms, including improvements to the tracking loop design to enable operation in HEO. These design changes are expected to allow modest reductions in the effective tracking threshold as compared with traditional receivers, which will translate into improved GPS signal visibility and improved navigation performance in the presence of poor GPS visibility.

In a highly eccentric orbit exhibiting poor GPS visibility throughout, navigation accuracies of better than 30 m and 2 mm/s RMS are achievable using a 35 dB-Hz threshold receiver. A 5 dB reduction in the tracking threshold was shown to improve these accuracies to better than 20 m and 1.2 mm/s RMS because of a corresponding increase in the number of visible GPS signals. In a geostationary orbit similar to the orbit of the GOES 10 spacecraft, navigation accuracies of better than 15 m and 1 mm/s RMS are achievable using a 35 dB-Hz threshold receiver. When the tracking threshold was improved by only 5 dB, these accuracies improved to better than 6 m and 0.4 mm/s RMS. With SA disabled, accuracies of better than 2 m RMS are achievable using a receiver with the reduced acquisition threshold.

The results suggest that the proposed receiver architecture will enable the use of GPS as an autonomous navigation sensor in HEO applications, satisfying a requirement for many future flight projects. Work is ongoing to further investigate the impact of using a lower-stability oscillator in the GPS receiver and to assess navigation performance for spacecraft orbits with even poorer GPS signal visibility, such as the 10×50 earth radii orbit proposed for the MMS mission (Table 1). These simulations were conducted prior to the discontinuation of SA on May 1, 2000; however, some discussion has been included as to how the results are likely to improve without SA. All future simula-

tions will be modeled with SA off. Some future work includes collecting experimental data on the long-term clock stability of the reference oscillator that will be used in the PiVoT receiver to verify the specified stability assumed in this analysis. Additionally, work is under way to verify the simulation results presented in this paper using actual GPS measurement data from the PiVoT receiver tracking satellites on the GPS constellation simulator at GSFC.

ACKNOWLEDGMENTS

The authors would like to acknowledge the significant contributions made by David Kelbel and Taesul Lee of Computer Sciences Corporation and Russell Carpenter of Goddard Space Flight Center to the work presented in this paper.

REFERENCES

1. Bauer, F. H. et al., *Enabling Spacecraft Formation Flying Through Spaceborne GPS and Enhanced Autonomy Technologies*, Proceedings of ION GPS-99, Nashville, TN, 1999.
2. Bell, E. V., *Imager for Magnetopause-to-Aurora Global Exploration (IMAGE)*, Last updated March 9, 2000, NASA Goddard Space Flight Center, <http://image.gsfc.nasa.gov/>.
3. *The Cluster II Mission: A Summary*, Last updated February 26, 1999, The European Space Agency, <http://sci.esa.int/missions/indexf.cfm?typeID=8&page=main&targetpage=www.estec.esa.nl/spdww/cluster/html2/mission.html>.
4. Williamson, P., *Phase 3D Project*, Last updated February 21, 2000, The Radio Amateur Satellite Corporation, <http://128.54.16.15/amsat/sats/phase3d.html>.
5. Issler, J. et al., *New Space GNSS Navigation Experiments*, Proceedings of ION GPS-99, Nashville, TN, 1999.
6. Rowland, D., *IMEX—Inner Magnetosphere Explorer*, Last updated February 25, 1999, University of Minnesota, <http://ham.space.umn.edu/spacephys/imex.html#Mission>.
7. Mauk, B. and B. Anderson, *Auroral Multiscale Midex (AMM)*, Accessed March 13, 2000, The Johns Hopkins University Applied Physics Laboratory, <http://sd-www.jhuapl.edu/AMM/>.
8. Neelon, J. et al., *Orbit Determination for Medium-Altitude Eccentric Orbits Using GPS*, AAS/AIAA Space Flight Mechanics Meeting, Breckenridge, CO, February 1999.
9. D'Mello, S., *Space Technology 5 (ST5)*, Last updated January 26, 2000, Jet Propulsion Laboratory, <http://nmp.jpl.nasa.gov/st5/>.
10. Personal communication with Dr. Steven A Curtis, Code 695, GSFC, June 14, 1999.
11. Brecker, K., *MMS: Magnetospheric Multi Scale*, Last updated February 11, 2000, NASA Goddard Space Flight Center, <http://mms.gsfc.nasa.gov/>.

12. *Magnetospheric Constellation*, Accessed March 13, 2000, NASA Goddard Space Flight Center, <<http://stprob.es.gsfc.nasa.gov/magcon.htm>>.
13. Yunck, T. P., *Orbit Determination*, Chapter 21 in B. Parkinson et al. (eds.), *Global Positioning System: Theory and Applications*, Vol. 2, Progress in Astronautics and Aeronautics, 1997, pp. 567–585.
14. Bisnath, S. B., *Spaceborne GPS Information Site*, Last updated August 19, 1999, Geodetic Research Laboratory, Department of Geodesy and Geomatics Engineering, University of New Brunswick, <http://gauss.gge.unb.ca/grads/sunil/sgps.htm>.
15. Wu, S. C., T. P. Yunck, S. M. Lichten, B. J. Haines, and R. P. Malla, *GPS Based Precise Tracking of Earth Satellites from Very Low to Geosynchronous Orbits*, National Telesystems Conference, 1992.
16. Ferrage, P., J. L. Issler, G. Campan, and J. C. Durand, *GPS Techniques for Navigation of Geostationary Satellites*, Proceedings of ION GPS-95, Salt Lake City, UT, September 1995, pp. 257–268.
17. Potti, J., P. Bernedo, and A. Pasetti, *Applicability of GPS-based Orbit Determination Systems to a Wide Range of HEO Missions*, Proceedings of ION GPS-95, Salt Lake City, UT, September 1995, pp. 589–598.
18. Spilker, J. J., *GPS Signal Structure and Theoretical Performance*, Chapter 3 in B. Parkinson et al. (eds.), *Global Positioning System: Theory and Applications*, Vol. 1, Progress in Astronautics and Aeronautics, 1997.
19. van de Pol, M., *YES-GPS*, Last updated April 21, 1998, European Space Research and Technology Centre, <http://www.estec.esa.nl/teamsat/page-menu_yes.html>.
20. Balbach, O. et al., *Tracking of GPS Above GPS Satellite Altitude: Results of the GPS Experiment on the HEO Mission EQUATOR-S*, Proceedings of ION GPS-98, Nashville, TN, 1998.
21. Belle G. et al., *The U.S. Air Force Academy GPS Flight Experiment Using the Navsys TIDGET*, Proceedings of ION GPS-97, Kansas City, MO, 1997.
22. Maki, S.C., *Optimization of a GPS User Experiment to GEO*, Proceedings of ION GPS-88, 1988.
23. Issler, J. L. et al., *High Reduction of Acquisition and Tracking Thresholds of GPS Spaceborne Receivers*, Proceedings of The Institute of Navigation 1998 National Technical Meeting, 1998.
24. Lightsey, E. G., *Development and Flight Demonstration of a GPS Receiver for Space*, Ph.D. Dissertation, Department of Aeronautics and Astronautics, Stanford University, February 1997.
25. Goddard Space Flight Center, Flight Dynamics Division, CSC-96-932-07R0UD0, *Global Positioning System (GPS) Enhanced Orbit Determination (GEODE) System Description and User's Guide*, Version 4, A. Long et al., prepared by Computer Sciences Corporation, February 1999.
26. B. Eissfeller, O. Balbach, and U. Rosbach, *GPS Navigation on the HEO Satellite Mission EQUATOR-S*, Results of the Feasibility Study, Proceedings of ION GPS-96, Kansas City, MO, 1996, pp. 1331–1340.
27. Goddard Space Flight Center, FDD/552-89/01, *Goddard Trajectory Determination System (GTDS) Mathematical Theory Revision 1*, A. Long et al., NASA Goddard Space Flight Center, June 1989.
28. Lear, W. M., *Range Bias Models for GPS Navigation Filters*, Charles Stark Draper Laboratory, June 1993.
29. Brown, R. G. and P. Y. C. Hwang, *Introduction to Random Signals and Applied Kalman Filtering*, Third Edition, John Wiley and Sons, 1997.
30. Czopek, F., *Description and Performance of the GPS Block I and II L-Band Antenna and Link Budget*, Proceedings of ION GPS-93, pp. 37-43.